Mathematical Clairvoyant: Mathematical Inverse Problems

Nathanael Ong
Arun Chakrabarty
Ashley Wang
Sarah Glomski

July 2021

1 Introduction

1.1 Overview

With current technology, we are able to utilize X-rays to obtain images of the human body. But an X-ray cannot just obtain a "picture" of internal objects inside the human body; how, then, do we obtain a legible image? When an X-ray beam passes through an object at a given intensity, a certain amount of the rays are absorbed or deflected by the object, which allows us to obtain information about the materials within the object. By examining that difference between the intensity of the X-rays that enter and exit, we can draw conclusions about the X-ray absorption of the materials in the body, which allows us to then reconstruct a sense of the materials that the X-rays had to pass through.

Computed tomography, more popularly known as CT scanning, is a medical imaging technique that obtains multiple X-ray measurements of the body from different angles and positions. With these measurements, computer algorithms can reconstruct cross-sectional "slices" of the body, as shown in Figure 1. Generally, X-rays are a minimally invasive way of imaging parts of the human body, with the CT scan being a particular applications that essentially collates multiple measurements into better, more high-construct results. However, the CT scan necessarily faces the mathematical problems related to reconstruction of an image from X-ray measurements. Beyond noise from scanning, the resulting reconstruction will not be perfect because mathematical reconstruction can only achieve an approximation of the actual object. Through understanding the mechanics behind the CT scan, we can also better understand possibilities for improving computer reconstruction.

In this paper, we will cover more of the background and properties of X-ray scanning, and discuss a number of computational reconstruction techniques that are used to obtain the actual "image" of a scanned object. We will further discuss a number of the issues and benefits related to each technique, and lastly explore the applications of these techniques to actual treatments using X-rays.

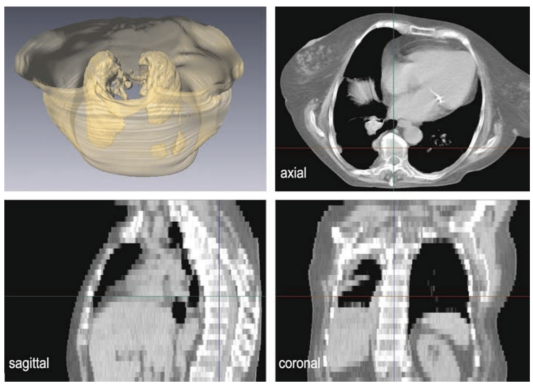

Figure 1: Examples of images obtained from CT scans (Buzug, 2008)

1.2 Relevant properties of the X-ray

Like all electromagnetic waves, x-rays have properties of both waves and particles. In the form of a wave, the energy of the beam is proportional to the frequency v by Planck's constant: $E = hv$. X-rays have very small wavelengths compared to visible light, and therefore have high frequencies and carry a high amount of energy.

In the form of particles, the energy of the beam is proportional to the number of particles present, or the intensity of the beam. When particles are shot through an object, some of them make it through while others get stuck inside the object, resulting in a loss of energy to the material. This energy loss can be measured by computing the difference in intensity of the x-rays before and after passing through the object, as shown in Figure 2.

Beer's Law states that the amount of energy lost to the material is proportional to the initial amount of energy that the beam has. This proportionality is represented by negative μ, which leads to an ordinary differential equation model. This will be discussed in more detail later on.

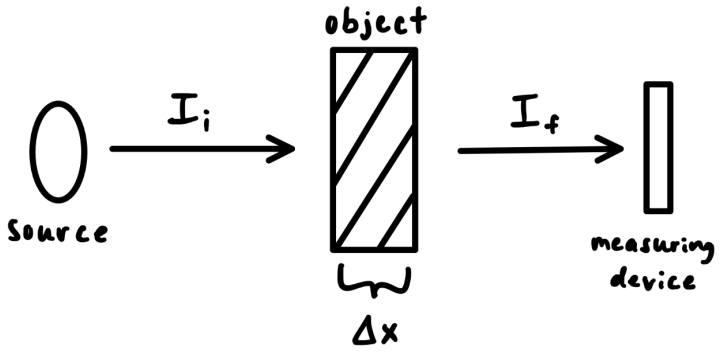

Figure 2: Energy transfer through an object

For the purposes of this paper, we will be assuming the usage of pencil-beam scanning, instead of other common techniques such as fan-beam scanning. Intuitively, the X-ray beam is very thin, resembling a pencil-beam, and each measurement gives a single value for the beam at its current position and angle. To

obtain full coverage of the object, the scanner is shifted horizontally in small increments for a total designated distance, then the scanner is rotated and this shifting is repeated. In most cases, this is repeated until all necessary points of the object of concern are illuminated by at least 180°. Mathematically, each pencil beam of the X-ray obtains a single value for the integral of the attenuation coefficient (μ) along a certain path through the object. Through shifting and rotating the scanner, we are able to obtain many values for these integrals which we can then use to aid a more accurate reconstruction of the requisite object.

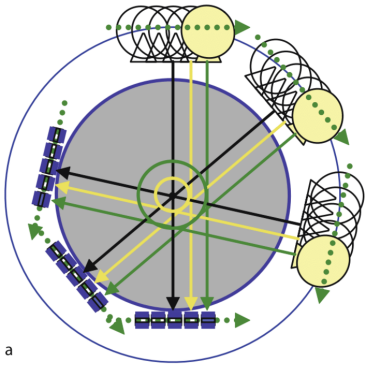

Figure 3: Pencil beam scanning setup (Buzug, 2008)

2 Mathematical Context

2.1 Ordinary Differential Equation Derivation

From Beer's Law comes the idea that an ordinary differential equation can model the change in energy associated with shooting a beam of x-rays through an object. The following equation can be used to represent the proportionality between the initial energy and change in energy after passing through an object:

$$\frac{I_f - I_i}{\Delta x} = -\mu I_i$$

Here, the *attenuation constant* μ represents the relative rate at which energy is absorbed at a certain point inside the material. μ is therefore a function of x, the position of the x-ray beam, and varies throughout the object.

In terms of calculus, this equation can be rewritten as the following:

$$\frac{dI(x)}{dx} = -\mu(x)I(x)$$

This equation is what's known as an *ordinary differential equation*, and can be solved the following way:

$$\begin{aligned}
\frac{dI(x)}{I(x)} &= -\mu(x)dx \\
\int_{in}^{out} \frac{dI(x)}{I(x)} &= -\int_{in}^{out} \mu(x)dx \\
[\ln I(x)]_{in}^{out} &= -\int_{in}^{out} \mu(x)dx \\
\ln I(out) - \ln I(in) &= -\int_{in}^{out} \mu(x)dx \\
\ln \frac{I(out)}{I(in)} &= -\int_{in}^{out} \mu(x)dx
\end{aligned}$$

We perform these operations in order to obtain the function $\mu(x)$, because theoretically if we can determine the attenuation at points within the material, it can help us determine the properties of the material itself. This is discussed in further detail in the next section.

Note that both $I(in)$ and $I(out)$ are measurable values, so the left hand side of this equation can be calculated experimentally and used to solve for $\mu(x)$ on the right hand side.

2.2 Radon Transform

Ideally, we would know the exact instance of $\mu(x)$ in any CT scan: i.e. we would know the attenuation coefficient at every position along the beam that passes through the object. If this was possible, we could more easily construct an image of the object: if we know the specific μ values for various materials, we could then know the span of each different material within the object. However, this is unmeasurable in reality. Instead, we define a function $g(x, y, \theta)$, that represents the integral of μ along a certain direction as described by the parameters.

$$\begin{aligned}
&\mu(x, y, \theta) \longmapsto g(x, y, \theta), \text{ where } g \text{ is defined as follows:} \\
&g(x, y, \theta) := \int_{in}^{out} \mu(x, y, \theta)ds
\end{aligned} \tag{1}$$

When we obtain x-ray measurements, we obviously do not just obtain values for μ along the line of the x-ray beam. Instead, when the detector receives the X-ray beam after a decrease in intensity, we can draw a conclusion about the overall μ that the beam must have passed through, which is represented in our function $g(x, y, \theta)$.

In practice and particularly in the examples we will use, we cannot truly represent our x-ray measurements with a continuous integral; instead, because we are scanning not continuously but in discrete steps, the integral will instead be a sum over those discrete steps. A perfect scanner would be able to cover both every scanning angle and obtain completely accurate values along every position at that scanning angle, but in reality we are dealing with a discretized version of these concepts. Though this necessarily results in an incomplete sampling of scanned objects, in practice this is usually sufficient to get a pretty good reconstruction of an object.

2.3 Parametrization of a Line

At a fixed angle θ, the straight-line path through the point (x_0, y_0) can be parameterized with a 2D vector $\vec{v}$ and parameter s, as shown in Figure 4. This parameterization is commonly referred to as *point-slope form* and is defined as follows:

$$x(s) = x_0 + s\cos\theta$$
$$y(s) = y_0 + s\sin\theta$$

Note that (x_0, y_0) is the initial point, $\vec{v} = (\cos\theta, \sin\theta)$ is the slope of the line, and $s \in \mathbb{R}$. In the context of the Radon Transform, this line parameterization can be used to modify equation (1) from above. The new equation for g is as follows:

$$g(x, y, \theta) := \int_{in}^{out} \mu(x_0 + s\cos\theta, y_0 + s\sin\theta)ds \tag{2}$$

However, this parameterization can be generalized even further by using two vectors to define the path instead of just one.

As before, the path is fixed at an angle θ with the horizontal, and the slope is given as $\vec{v} = (\cos\theta, \sin\theta)$. But now, a position vector $\vec{r}$ points from the origin O to the point (x_0, y_0) such that it forms a right angle with vector $\vec{v}$, as shown in Figure 4.

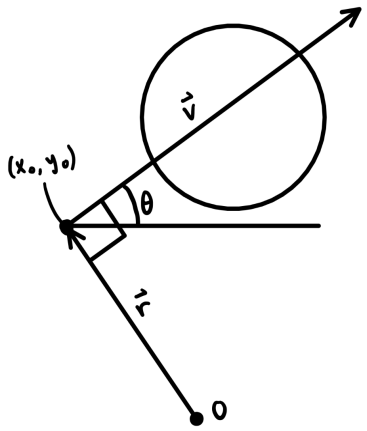

Figure 4: 2D parameterization of a line (vector form)

Given this geometric setup, it can be deduced that $\vec{r} = (-\sin\theta, \cos\theta)$, and if the magnitude of $\vec{r}$ is defined to be r, a real number, then a new equation for g can be written in terms of r and θ as follows:

$$g(r, \theta) := \int_{in}^{out} \mu(-r\sin\theta + s\cos\theta, r\cos\theta + s\sin\theta)ds \tag{3}$$

r and θ can be used to differentiate between the beams that pass through the object when using the pencil beam technique. Each individual beam possesses a unique combination of the starting point and angle at which it is shot, justifying our ability to define a complete parameterization in terms of these variables.

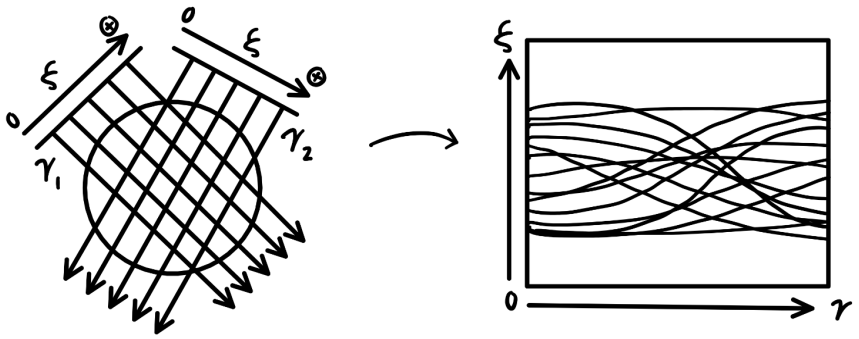

Figure 5: Sinogram resulting from pencil beam scanning technique

Above, we have illustrated a brief example that displays the visualization of individual X-ray beams in terms of these parameters. The image on the right is often referred to as a *sinogram* due to how objects can result in sinusoidal patterns on the graph. In fact, if this method of pencil-beam scanning was performed on a single dot of nonzero μ in the xy-coordinate system, the "sinogram" would just appear to be a sine wave. The sinogram displayed in the above right graph is "built" from left to right, and is a display of what would occur if the scanner was fully rotated around the scanned object shown on the left.

Figure 5 is a simple graphical example of a possible sinogram, and shows how more complex sinograms are in effect "layerings" of objects that appear on the sinogram because of their contrasting attenuation coefficients. If we recall that a single dot would result in a single sine wave, we can then observe how each separate line in the sinogram represents a distinct object that is represented by a sinusoidal trace.

Below, we have another graphical example of sinograms that resulted from a scan of an abdomen, with an additional representation on a polar grid. Sinograms are "brightest" when the corresponding beam detects relatively higher attenuation. From the information obtained from X-ray scanning that is then displayed in the Radon space, we are able to proceed with various techniques of reconstruction.

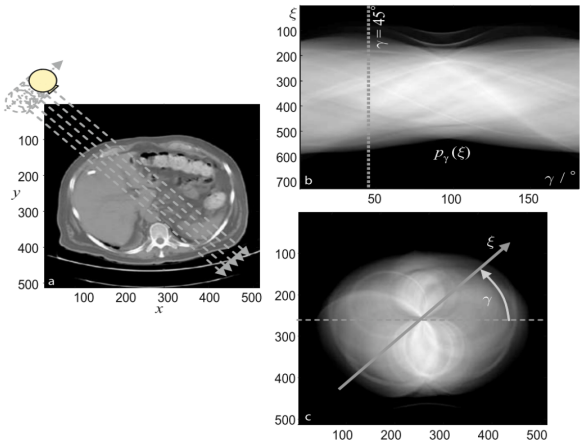

Figure 6: Cartesian and polar sinograms resulting from an abdominal CT scan (Buzug, 2008)

3 Code Implementation of the Radon Transform

```
def line_integral(f,s,theta):
  N = len(f)
  pts = int(np.ceil(2*np.sqrt(2)*N))
  t = np.linspace(-np.sqrt(2),np.sqrt(2),num=pts)
  x = s*np.sin(theta)+t*np.cos(theta)
  y = -s*np.cos(theta)+t*np.sin(theta)
  cols = np.floor(x*N/2)+N/2
  rows = np.floor(y*N/2)+N/2-1
  v = np.zeros(pts,dtype=object)
  for i in range(pts):
    v[i] = (rows[i],cols[i])
  vset = list(set(v))
  rsum = 0
  for tup in vset:
    if tup[0]>=0 and tup[0]<N and tup[1]>=0 and tup[1]<N:
      rsum += f[int(tup[0])][int(tup[1])]
  return rsum

def radon_transform(f,n=180):
  N = len(f)
  pts = int(np.ceil(2*np.sqrt(2)*N))
  theta = np.linspace(0,np.pi,n)
  s = np.linspace(-np.sqrt(2),np.sqrt(2),pts)
  I = np.zeros(shape = (pts,n))
  for i in range(pts):
    for ii in range(n):
      I[i][ii] = line_integral(f,s[i],theta[ii])
  return I
```

Figure 7: Radon Transform Implementation

For this implementation, we first considered a grid on the xy-plane with x and y values ranging from $-\sqrt{2}$ to $\sqrt{2}$. We then considered lines passing through this grid at various r and θ values and computed the line integral using the function above. Finally, the results were then returned in a matrix consisting of these values on the $r-\theta$ plane with the following results on the right:

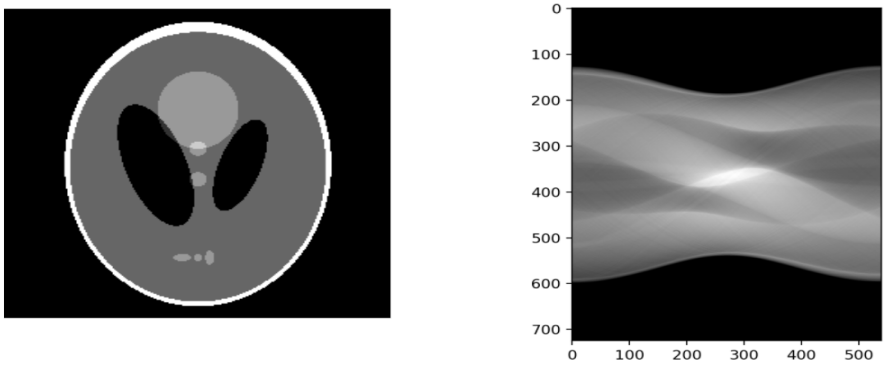

Figure 8: Results of Radon Transform using the Shepp Logan Phantom

4 Analytic Image Reconstruction

A CT scan performs a radon transform over a discrete image matrix representing the patient data. In order to recover the image of the target tissue using analytical methods, it is necessary to know the inverse of the radon transform.

4.1 Backprojection

Starting with the definition of the radon transform $Rf : \mu(x, y) \to g(r, \theta)$.

$$g(r, \theta) = \int_{-\infty}^{\infty} \mu(-r \sin\theta + s \cos\theta, r \cos\theta + s \sin\theta) ds$$

Choose a path p through the area of interest. The attenuation of the x-ray in one direction of p is the same as the attenuation in the opposite direction. Define $\bar{\mu}$ as the constant average attenuation along a path. Assume $\bar{\mu}$ can be used to approximate the function μ along the path, then simplify the radon transform:

$$g(r, \theta) = \int_p \bar{\mu} ds$$

Integration of a constant implies $g(r, \theta) \propto \bar{\mu}$, however the constant of proportionality is often ignored, so $\bar{\mu} = g(r, \theta)$. To solve the attenuation at a single point (x, y), take the average of $\bar{\mu}$ along all paths crossing through (x, y). The path angle varies from 0 to π.

$$\tilde{\mu}(x, y) = \frac{1}{\pi} \int_0^{\pi} g(r, \theta) d\theta$$

Solve for the parameter r in terms of the relevant variables x, y, θ using the Radon transform expressions for x, y.

$$x = -r \sin\theta + s \cos\theta \implies x \sin\theta = -r \sin^2\theta + s \cos\theta \sin\theta$$

$$y = r \cos\theta + s \sin\theta \implies y \cos\theta = r \cos^2\theta + s \sin\theta \cos\theta$$

Therefore,

$$y \cos\theta - x \sin\theta = r(\sin^2\theta + \cos^2\theta) = r$$

Substitute to arrive at backprojection integral,

$$\tilde{\mu}(x, y) = \frac{1}{\pi} \int_0^{\pi} g(y \cos\theta - x \sin\theta, \theta) d\theta$$

The backprojection integral, which maps $g(r, \theta) \to \mu(x, y)$, from Radon space to image space, is necessary for analytic reconstruction.

4.2 Backprojection Filtered (BPF)

Observing the reconstruction in figure 7, the $\tilde{\mu}$ recovered from simply feeding the sinogram data into the backprojection integral is blurry and inaccurate. This makes it insufficient for clinical use. In order to achieve

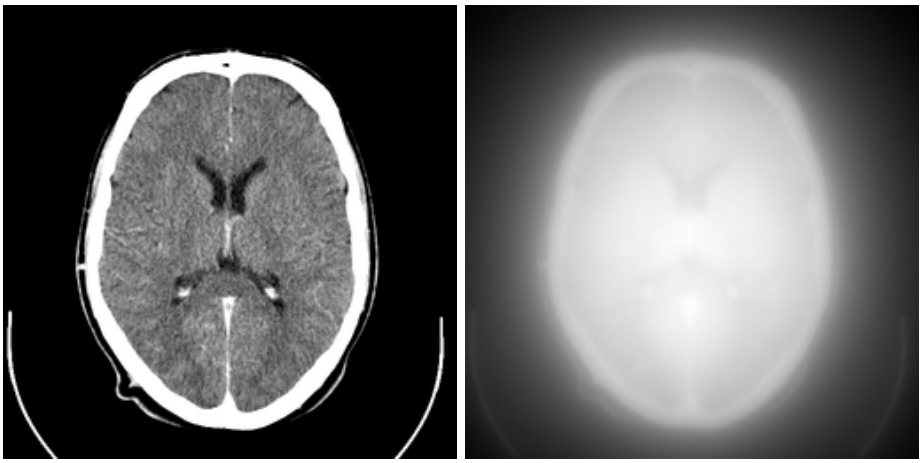

Figure 9: Left: Sample image used to generate a sinogram, Right: Reconstructed image using only backprojection

sharper image reconstruction and better feature identification, it is necessary use the Fourier transform to reduce noise.

Start with the backprojection integral. Use the Radon transform integral to rewrite the backprojection integral.

$$\tilde{\mu} = \frac{1}{\pi}\int_0^{\pi}\int_{-\infty}^{\infty} \mu(-r\sin\theta + s\cos\theta, r\cos\theta + s\sin\theta)dsd\theta$$

Apply change of variables to rewrite in terms of $s' = s - (x\cos\theta + y\sin\theta)$. Rearrange

$$s = s' + (x\cos\theta + y\sin\theta)$$

Earlier it was shown that $r = y\cos\theta - x\sin\theta$. Substitute for s and r in the integral above. After some work, we get

$$\tilde{\mu}(x,y) = \frac{1}{\pi}\int_0^{\pi}\int_{-\infty}^{\infty} \mu(s'\cos\theta + x, s'\sin\theta + y)ds'd\theta$$

Now change variables from polar to cartesian. Let $w = s'\sin\theta$ and $z = s'\cos\theta$. We know

$$dwdz = s'ds'd\theta \implies ds'd\theta = \frac{1}{s'}dwdz$$

Write s' in terms of w, z:

$$w^2 + z^2 = s'^2(\cos^2\theta + \sin^2\theta) = s'^2$$
$$\implies s' = \sqrt{w^2 + z^2}$$

Therefore,

$$\tilde{\mu}(x,y) = \frac{1}{\pi}\int_{-\infty}^{\infty}\int_{-\infty}^{\infty} \mu(z+x, w+y)\frac{1}{\sqrt{w^2+z^2}}dwdz$$

This is a 2-D convolution integral, hence apply the definition

$$\tilde{\mu}(x,y) = \frac{\mu}{\pi} * \left(\frac{1}{\sqrt{x^2+y^2}} \right)$$

Apply the convolution theorem,

$$\tilde{\mu} = \frac{1}{\pi} \mathcal{F}\mu \cdot \mathcal{F} \left(\frac{1}{\sqrt{x^2+y^2}} \right)$$

Solve for μ and use a reference table,

$$\mu = \mathcal{F}^{-1} \left[\tilde{\mu}(k_1,k_2) \cdot \sqrt{k_1^2+k_2^2} \right]$$

To perform BPF, first feed the sinogram into backprojection, then take the 2D Fourier transform, then multiply by the frequency domain filter, and finally take the inverse 2D fourier transform.

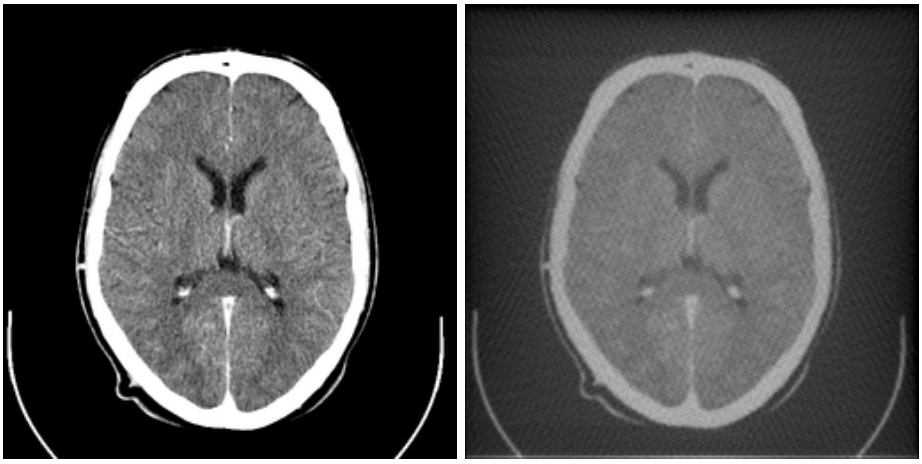

Figure 10: Left: Sample image used to generate a sinogram, Right: Reconstructed image using BPF

4.3 Filtered Backprojection (FBP)

Another analytic reconstruction method makes use of the Fourier Slice Theorem. To derive the Fourier Slice Theorem, start by taking the 1D Fourier transform of g with respect to r and substitute the integral form of g.

$$\mathcal{F}g(k) = \int_{\infty}^{\infty} g(r,\theta) e^{-ikr} dr$$

$$= \int_{\infty}^{\infty} \left(\int_{\infty}^{\infty} \mu(-r\sin\theta + s\cos\theta, r\cos\theta + s\sin\theta) ds \right) e^{-ikr} dr$$

Using the change of variables $x = -r\sin\theta + s\cos\theta$ and $y = r\cos\theta + s\sin\theta$, rewrite the integral. The Jacobian of transformation is $cos^2\theta - (-\sin^2\theta) = 1$. Rewrite the integral

$$\mathcal{F}g = \int_{\infty}^{\infty} g(r,\theta) e^{-ikr} dr$$

$$= \int_{\infty}^{\infty} \int_{\infty}^{\infty} \mu(x,y) e^{-ik(y\cos\theta - x\sin\theta)} dxdy$$

This is a 2D Fourier Transform. Therefore

$$\mathcal{F}_{1D}[g(k,\theta)] = \mathcal{F}_{2D}[\mu](k_1,k_2) = \mathcal{F}_{2D}[\mu](-k\sin\theta, k\cos\theta)$$

Now starting with the equation

$$\mu(x,y) = \mathcal{F}_{2D}^{-1}[\mathcal{F}_{2D}[\mu]]$$

Apply definition of inverse 2D Fourier transform, then perform necessary substitutions and change to polar coordinates.

$$\mu(x,y) = \frac{1}{\pi} \int_0^{\pi} \int_{-\infty}^{\infty} \mathcal{F}_{2D}[\mu](-k\sin\theta, k\cos\theta) e^{i[-k\cos\theta x + k\sin\theta y]} |k| dkd\theta$$

Substitute the the Fourier Slice Theorem result for $\mathcal{F}_{2D}[\mu]$ and simplify by recognizing an inverse 1D Fourier transform integral. The $|k|$ term multiplies with the 1D Fourier transform of g, and acts as a low-pass filter step.

$$\mu(x,y) = \frac{1}{\pi} \int_0^{\pi} \mathcal{F}_{1D}^{-1} \left[\mathcal{F}_{1D}[g](k,\theta)|k|\right] (-x\cos\theta + y\sin\theta) d\theta$$

Recognize this is the backprojection integral. Let Rf^{-1} represent the Radon transform inverse operator, which is backprojection.

$$\mu(x,y) = Rf^{-1}\left[\mathcal{F}_{2D}^{-1}\mathcal{F}_{1D}[g](k,\theta)|k|\right]$$

The formula above demonstrates the difference between BPF and FBP is when the backprojection algorithm is called. Recall in BPF the first step is to backproject, followed by taking the Fourier transform, filtering, and taking the inverse Fourier transform. By contrast, in FBP the first step is taking a Fourier transform, then filtering and taking the inverse transform, then calling backprojection. This subtle difference has noticeable effects in improving image quality, as shown figure 10. In summary, two analytic methods of

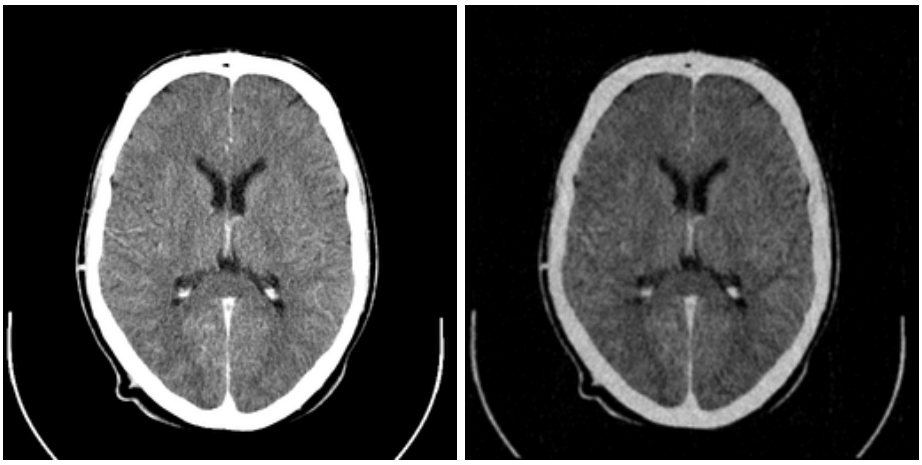

Figure 11: Left: Sample image used to generate a sinogram, Right: Reconstructed image using only FBP

image reconstruction from a CT sinogram were discussed: BPF and FBP. BPF and FBP differ in the order of backprojection and spectral filtering steps, which is shown to impact the reconstructed image quality.

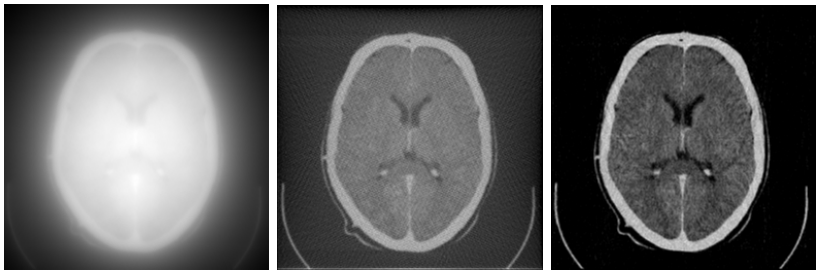

Figure 12: Side-by-side comparison of (Left to Right) Backprojection, BPF, FBP

5 Algebraic Reconstruction Technique (ART)

Given stability issues with regards to the inverse radon transform, the FBP and BPF are likely to be infeasible given noises in the data g or discontinuity in μ. Hence, the resulting reconstruction is likely to have some artificial effects. The ART is the most commonly use method to reduce these effects by creating a system matrix and solving the linear equation $Ax = b$

5.1 Creating the System Matrix

For each ray p_1, p_2, p_3, p_4 shown in this diagram, each is associated with a value of $g(r, \theta)$ which is the result of the radon transformation. The distance of each ray through each grid is put into matrix A as a weight.

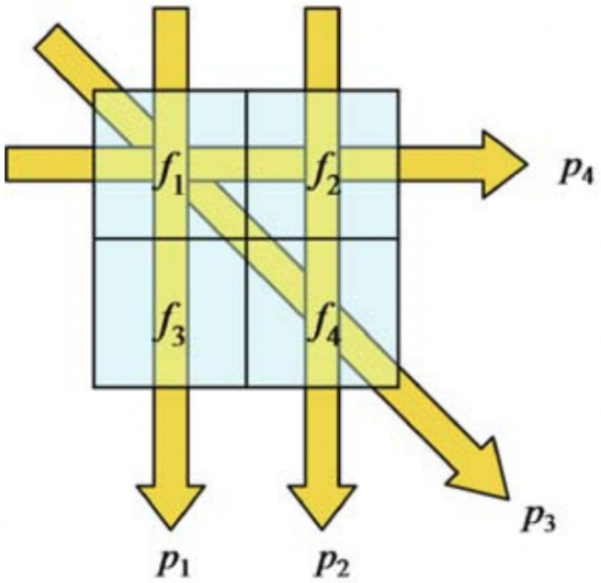

Figure 13: ART illustration

More generally, let μ be the absorption coefficient image with NxN pixels and we assume the μ to be constant on each pixel. Then we assign μ_{ij} to each pixel for $1 \leq i, j \leq N$. For each line determined by r and θ, it

will pass through some of these pixels and take the path length inside each pixel to be p_{ij}. If the line does not pass through the pixel, then $p_{ij} = 0$. So the equation for the $(k, s)^{th}$ line given by parameter (r_k, θ_s) is given by

$$\sum_{i,j} \mu_{ij} p_{ij}^{k,s} = g(r_k, \theta_s)$$

where p_{ij} is determined by the straight line (r_k, θ_s), and the entries of $A_{(k,s),(i,j)}$ will be $p_{ij}^{k,s}$. Overall, A is a MxN^2 matrix where $M \geq N^2$ in order to create an overdetermined system with a unique solution. x is the vectorized form of a NxN matrix while b is a Mx1 vector.

5.2 Solving the System

Given that the matrix A is often a singular matrix, the goal would be to find a least square solution and minimize $|Ax - b|^2$ rather than explicitly solving for x. For this the Kaczmarz's method, an iterative algorithm given by:

$$x^k = x^{k-1} - \frac{A_i x^{n-1} - b_i}{A_i A_i^T} A_i^T \ (*)$$

where A_i is the i-th row of the matrix A, and the iteration number k satisfies i=k mod $N^2 + 1$

Proof : Left multiply both sides of (*) by A_i, we get the equation

$$A_i x^k = A_i x^{k-1} - \frac{A_i x^{n-1} - b_i}{A_i A_i^T} A_i A_i^T$$

Cancelling and subtracting terms we get

$$A_i x^k = b_i$$

as required

5.3 Comparing ART and FBP

ART produces a much higher quality image as compared to FBP. ART also allows for more flexibility in terms of one's ability to alter the technique to improve image quality However, ART has a much longer runtime and is more computationally expensive. During our trials, ART took around 30 minutes to run on average, whereas FBP took only about 5 minutes on average. Hence, FBP is still the most popular method used in industry.

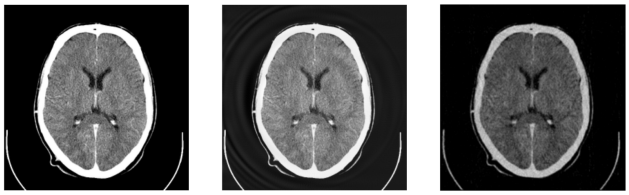

Figure 14: Comparison of images from ART and FBP

6 Interpolation

In order to improve the resolution of ART, we must change the way that the code simulates collecting the attenuation data.

Currently, in order to simulate a single x-ray beam, the code basically "drops" a bunch of points onto the starting image, then figures out which cell of the matrix those points "fell into". Using the nearest neighbor technique, each point is assigned the value of the cell it fell into, which makes the assumption that the attenuation is constant throughout the entire cell. This assumption introduces error to the data, however, because the attenuation of tissue in real life is continuous, not discrete. Thus, the goal is to make it continuous using interpolation.

With interpolation, instead of using the nearest neighbor, the code operates on the assumption that the point's value is some linear combination of its four nearest neighbors' values. Thus, linear algebra can be used to better approximate the value at the point. We set up a system of equations using the following bilinear approximation equation: p(x, y) = axy + bx + cy + d

Again, this is simply showing that the point p is some linear combination of its four nearest neighbors, each given a weight *a*, *b*, *c*, or *d*. The linear system follows:

$$\begin{cases} f(0,0) = d \\ f(1,0) = b + d \\ f(0,1) = c + d \\ f(1,1) = a + b + c + d \end{cases}$$

Using this setup, the following Python code manually (and efficiently) solves the system and returns the weights *a*, *b*, *c*, and *d*. From there, the point value is calculated using a weighted average.

Now, instead of assuming that each cell has a constant value, the code is able to construct a set of planes between each cluster points, which allows for a more accurate approximation. However, the interpolation method is not able to add any new information to the data. For instance, if a small feature was missed during data collection, interpolation will not be able to fill in the gaps to find it. Overall though, it is still a useful method for making the final CT images appear less granular, which is more pleasant to the eye.

```
# Square interpolation function

# param
#   f00,f10,f01,f11: four corner values
# return: numpy vector (a,b,c,d)

def squareInterp(f00,f10,f01,f11):
  # write system of eq as matrices
  A = np.array([[0,0,0,1],[0,1,0,1],[0,0,1,1],[1,1,1,1]])
  b = np.array([f00,f10,f01,f11])

  # solve Ax = b manually
  d = f00
  b = f10-d
  c = f01-d
  a = f11-b-c-d
  return [a,b,c,d]
```

Figure 15: Interpolation code

7 Region of Interest Isolation

The next goal for improving ART is to be able to isolate just one region of interest (or ROI), because many times when we scan the human body, we only care about a small portion of it, such as where a tumor is located. Thus, we want to be able to increase the resolution of the image within that region of interest.

On the other hand, x-rays are very harmful to human tissue, so if we are targeting a tumor through radiation therapy, we want to ensure that there's no unnecessary damage to the surrounding tissue. Therefore, the goal is to find the balance between too high of a dosage and too low of a dosage.

7.1 Naive Approach

The naive approach was to restrict the x-ray beams so that they only go through the ROI, and then use regular ART to reconstruct the ROI. However, this led to an inaccurate reconstruction, which was very dark and had a poor resolution. This was due to the fact that when we took the scan, the surrounding tissue was interfering with the attenuation data, causing it to appear denser than it actually was. From here, we had to create a more complex method–one that requires two CT scans–in order to achieve a better reconstruction.

7.2 Dual Scan Method

First, a low dose CT scan is performed, which generates a coarse image. This first scan does minimal damage to the tissue while still allowing us to locate the region of interest.

From there, we isolate the beams that actually intersected with the ROI and calculate what percentage of

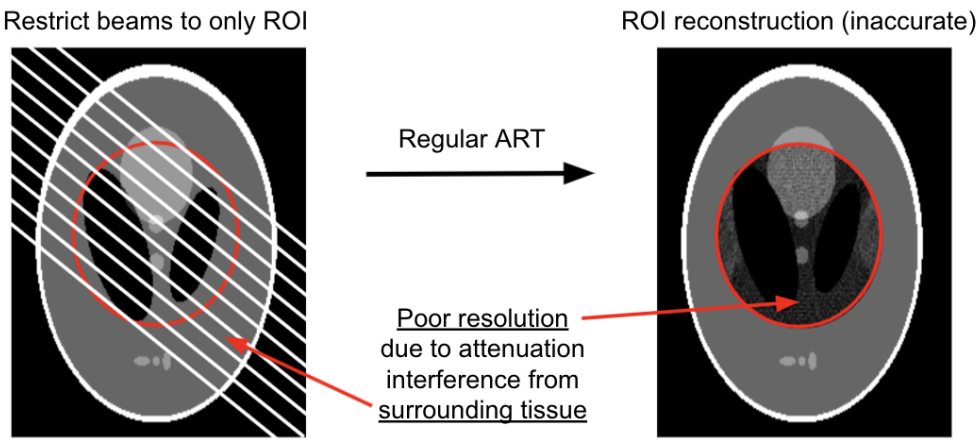

Figure 16: Naive approach to ROI reconstruction

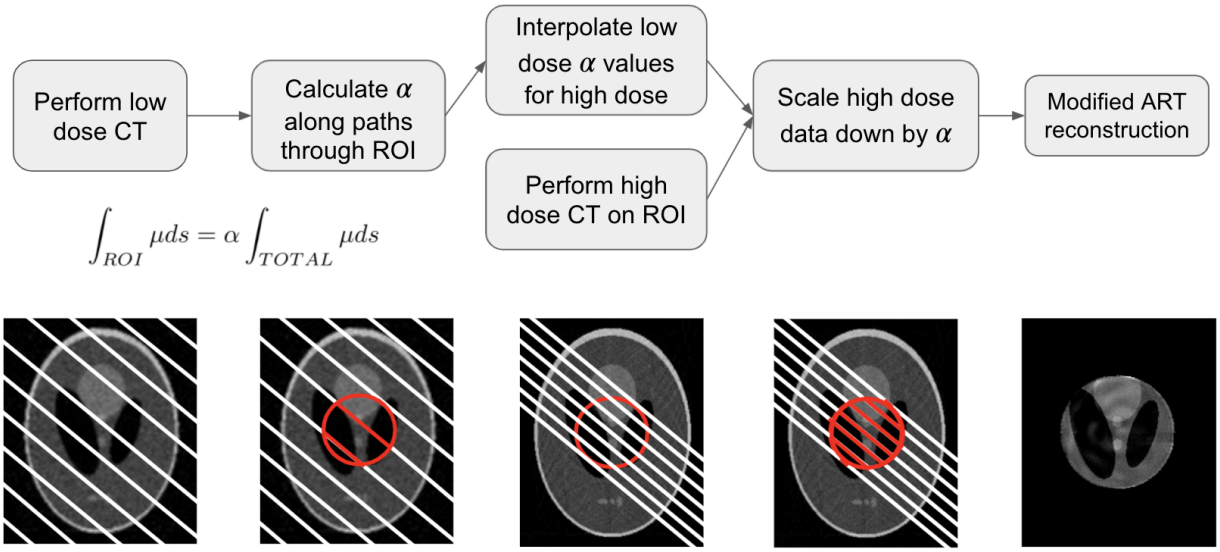

Figure 17: Dual scan method for ROI reconstruction

them fell inside the ROI (see red line segments in the second image.) That percentage of the line is called α, and we intend to store these α values for later, because we assume that this ratio will stay relatively constant between the first and second CT scans.

Next, a high dose CT scan is performed on only the region of interest. Now we interpolate the low-dose alpha values so that there's one alpha value for each beam. This indicates how much of that beam actually falls within the ROI, which allows us to scale down the data from our high dose CT scan so that it's only accounting for the attenuation within the ROI. Finally, a modified version of ART is used to reconstruct the ROI.

7.3 Low Dose Interpolation Method

This second method first halves the resolution in each r and θ direction, resulting in the low dose CT having $\frac{1}{4}$ the resolution or dose of the normal ART. The region of interest in blue was then isolated. High resolution CT amounting to a resolution 4 times that of the low dose CT in the θ direction was then directed at the region of interest. This resulted in a clearer region of interest but a less clear image outside the region of interest as compared to the previous ART as expected. In particular, the white circular boundary of the shape was not as clear.

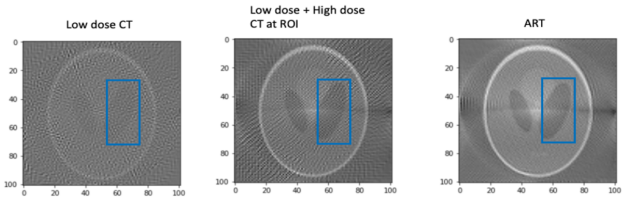

Figure 18: Low Dose Interpolation Results

8 Inverse Planning

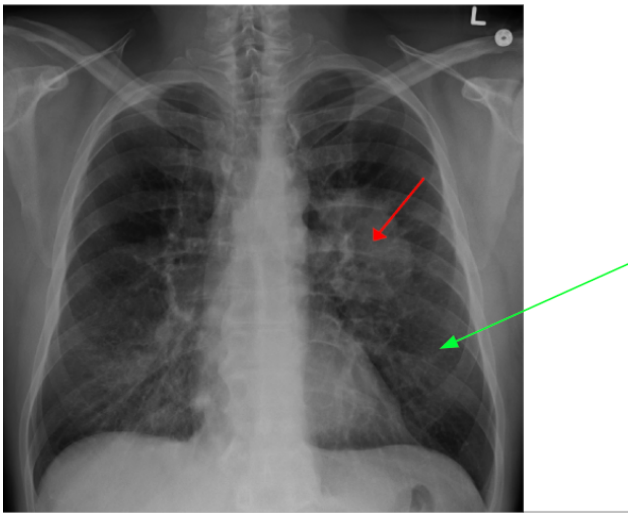

Figure 19: Image of Lungs with Tumor Region as ROI

Once the imaging is completed, the next phase is the treatment phase and the challenge is to optimize the dose of radiation given to the patient during radiotherapy. The aim is to keep the radiation dose within a certain limit in the ROI and below a certain limit outside the ROI, giving rise to the following system that can be solved using linear programming techniques:

$$R_T^L \leq \sum_i \lambda_i B_i x_T \leq R_T^U \text{ (ROI)}$$

$$\sum_i \lambda_i B_i x_N \leq R_T^N \text{ (Outside ROI)}$$

$$\lambda_i \geq 0$$

where R_T^L and R_T^U are the lower and upper bounds of radiation dose for the ROI, R_T^N is the upper bound of radiation dose for the non-ROI, B_i is the i^{th} row of the B system matrix, λ_i is the radiation dose we are trying to optimize. x_T is the the indicator function written in the form of a vector with elements 1 indicating the position of the ROI and 0 otherwise. The converse is true for x_N.

This system is often solved using the Simplex Method. However, it is usually infeasible and penalty terms would have to be added to create a solvable system as shown below:

$$R_T^L - \alpha \leq \sum_i \lambda_i B_i x_T \leq R_T^U + \beta \text{ (ROI)}$$

$$\sum_i \lambda_i B_i x_N \leq R_T^N + \gamma \text{ (Outside ROI)}$$

$$\lambda_i \geq 0$$

9 Conclusion

This project examined the mathematics of x-ray CT, radon transform, and various image reconstruction techniques and created 2 new ways which would improve the scanning process- the dual scan method and the low dose interpolation method. Given the better precision and greater flexibility of the dual scan method, it would be reasonable to conclude that this method would likely form the basis for future research. Going forward, we hope to further develop the methods for interpolation and finding the variation of μ within each square grid. This would involve a more in depth study into how X-rays attenuate through different materials and how PDE models can be used to model the variation of intensity of an X-ray through different matter.

References

Buzug, T. (2008). Computed Tomography. Springer-Verlag Berlin Heidelberg.